Influence of particle size distribution on the mechanical behavior of a soil

Philippe REIFFSTECK*
Phuong-Thao NGUYEN PHAM
Université Paris-Est,
Laboratoire central des ponts et chaussées,
Paris, France

Jocelyn ARBAUT
Centre d'études techniques de l'équipement
Normandie-Centre,
Le Grand Quevilly, France

ABSTRACT

Understanding the behavior of heterogeneous soils requires knowledge of the influence from particle size distribution on the mechanical parameters. The results derived from tests conducted on a sand sample and glass beads of four different diameters, mixed in various proportions so as to recreate a particle size distribution curve, will be presented herein. Mixes involving kaolinite and Fontainebleau sand have also been studied in order to evaluate the influence of fine and coarse particle proportions on the mechanical strength of the final mix. An analysis of results from shear strength measurements leads to proposing the following interpretation: materials displaying a hollow particle size distribution curve, i.e. concave towards the top, have a higher optimal density and hence particles fit together more tightly. Consequently, greater shear strength is observed for these materials. It seems plausible that the same reasoning could also apply to deformation behavior. The validation of a mix-type model lying within the family of critical state models was also undertaken, first for a series of model materials then for materials composed of varying particle size fractions with both a Seine River alluvial gravel and rock debris from the natural slopes of the *La Maurienne* Valley (French Alps).

Influence de la répartition granulométrique sur le comportement mécanique d'un sol

RÉSUMÉ

La compréhension du comportement des sols hétérogènes impose de connaître l'influence de la distribution granulométrique sur les paramètres mécaniques. Les résultats d'essais effectués sur un sable et des billes de verre de quatre diamètres, mélangés en différentes proportions de manière à recréer une courbe granulométrique, sont présentés. Des mélanges de kaolinite et de sable de Fontainebleau ont été également étudiés afin d'évaluer l'influence des proportions en particules fines et grossières sur la résistance mécanique du mélange. L'analyse des résultats des mesures de résistances au cisaillement conduit à proposer l'interprétation suivante : les matériaux dont la courbe granulométrique est creuse, c'est-à-dire concave vers le haut, présentent un optimum de densité plus élevé et donc un engrènement meilleur des particules. De ce fait, on peut observer pour ces matériaux une résistance au cisaillement supérieure. Il semble qu'il en soit de même pour le comportement en déformation. La validation d'un modèle de type mélange s'inscrivant dans la famille des modèles d'état critique a été ensuite réalisée pour les matériaux modèles, puis pour des matériaux composés de différentes fractions granulométriques d'une grave alluvionnaire de la Seine et d'éboulis des versants naturels de la Maurienne.

*** Corresponding author:**
Philippe REIFFSTECK
philippe.reiffsteck@lcpc.fr

INTRODUCTION

Soils result from the disaggregation and alteration of rocks due to various factors and have often been exposed to transport. Heterogeneous soils constitute a special category of soil; they display a complex grain size distribution due to a composition consisting of coarse elements (greater than

50 mm) positioned within a fine soil matrix **[1]**. They are frequently encountered in civil engineering works, in particular in road and rail infrastructure projects, either as foundation soil for structures or earthworks or as reused backfill soil. One of the major problems tied to use of these soils is the characterization of their mechanical behavior. The limitation in test equipment dimensions prevents the laboratory testing of particle sizes typically in excess of 25 mm **[2]**. The approach that makes use of databases and correlations has not yet reached a sufficient level of sophistication to be usable **[3]**. The possibility of determining material behavior by means of testing just a narrow particle size range thus remains vital as a practical approach.

Research has demonstrated that once the percentage of fines in a given material has reached a value of 70% to 80%, mix behavior is dominated by the fines composition. Below this value, its behavior is mixed, and beneath a threshold consisting of between 20% and 30% fines, mix behavior becomes governed by the coarse fraction.

This phenomenon has been observed with greater precision in mixes composed of spherical particles of two different sizes. In this special case, the arrangement is affected by the proportions of large-diameter and small-diameter spheres as well as by the ratio of the large sphere diameters to the small sphere diameters **[4-7]**.

The examination herein will focus first on variation in the densest state (e_{min}: minimum void index) with respect to the proportion of the fine fraction.

Figure 1a diagrams how void and solid volumes evolve with the percentage of fines. Point L on the diagram represents the densest assembly of coarse particles. At the beginning, the addition of fines into this dense state of coarse particles leads to a reduction in void volume until a point when fines fill the voids: this corresponds to Phase LT **(see Fig. 2)**. The addition of fines beyond point T causes the reverse trend, i.e. the void volume increases with the percentage of fines. During this Phase TS, the coarse particles no longer touch one another, move apart from one another and get embedded in the fines matrix until disappearing at Point S **(Fig. 1b)**.

Changes in the minimum void index e_{min} corresponding with this process has been depicted on **Figure 1b**. The minimum value of this index is obtained for a fines content well below 50% and

figure 1
Effect of fines on a sphere assembly:
- a: Evolution in proportions of the various particle fractions
- b: Evolution in void index of the mix (extracted from **[5]***)*

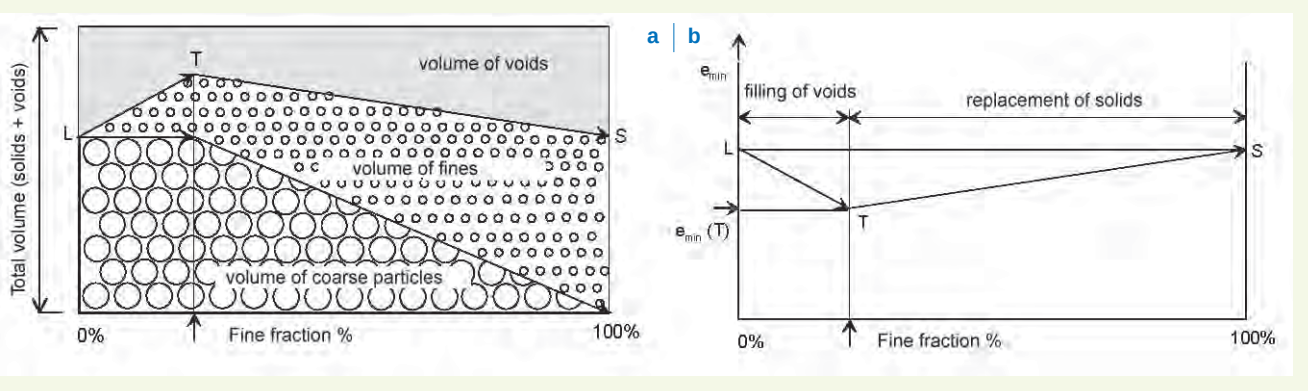

figure 2
Effect of fines on a sphere assembly (extracted from **[5]***)*

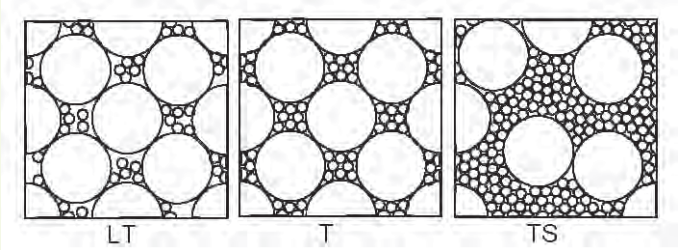

estimated at approximately 30%. This void index varies between minimum and maximum values, as defined by the constituent materials.

As indicated above, the relative size of both the large and small spheres constitutes another factor influencing the mix of these two groups. It appears that the small spheres may be included among the larger ones if the diameter of the larger spheres is at least 6.5 times greater than that of the smaller ones, i.e. if $d_{large} > d_{small}.6.5$, as illustrated in **Figure 3b**.

$$d_{large} = 2.\left(\frac{d}{2}.\frac{1}{\cos 30} - \frac{d}{2}\right) = \left(\frac{2}{\sqrt{3}} - 1\right).d = \frac{1}{6,464}.d_{small} \quad (1)$$

The behavior shown on **Figure 3b** can be compared to evolutions in the minimum and maximum void index vs. the d_{60}/d_{10} ratio previously proposed **[8]**. The threshold suggested by these authors is situated at a value equal to 10.

In this regard, it is to be recalled that void index evolution vs. particle size categories for a mix can be derived by observing the shape of the particle size distribution curve. As a matter of fact, if it were presumed that each particle size class removed by a ratio equal to 6.5 only makes up 30% in volume terms of the next higher class, then a polyline very similar to that proposed by Fuller and Thompson will be obtained for the same objective. These authors had proposed a particle size distribution curve based on experimental findings, which has since been called the Fuller curve, that yields the maximum grain arrangement **[9]** **(see Figs. 4** and **5)**.

Similar analyses were conducted in the area of concrete mix design and have led to a set of sophisticated tools for predicting the compactness of granular mixes: the granular stacking model **[10]**. What actually inspired this research however was the proposal by various authors of a similar evolution for the modulus of deformation, angle of internal friction and for physical characterization parameters like the Atterberg limits **[4,11-19]** **(Figs. 6a** and **6b)**.

figure 3
Effect of the percentage of fines and ratio of coarse and fine particle diameters to the void index **[5]**

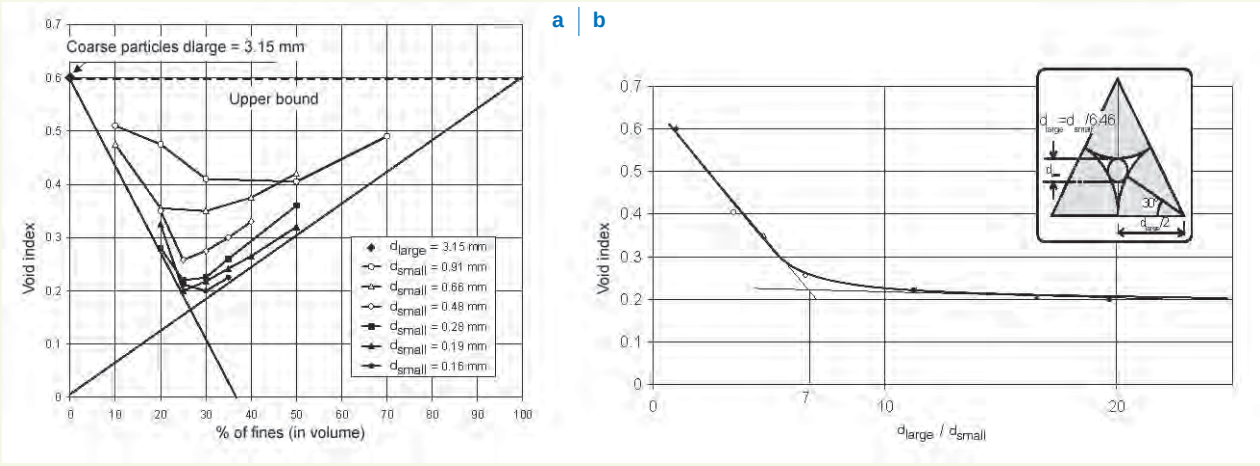

figure 4
Fuller's idealized arrangement and the corresponding particle size distribution curve equation

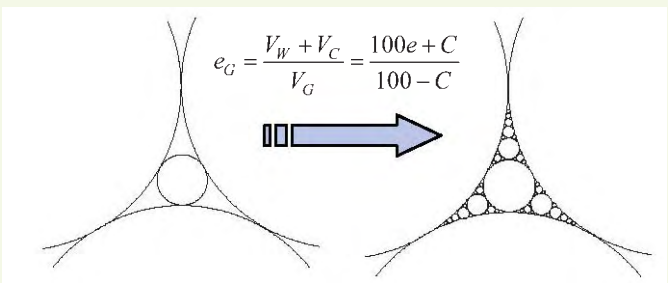

figure 5
So-called Fuller curve and polyline

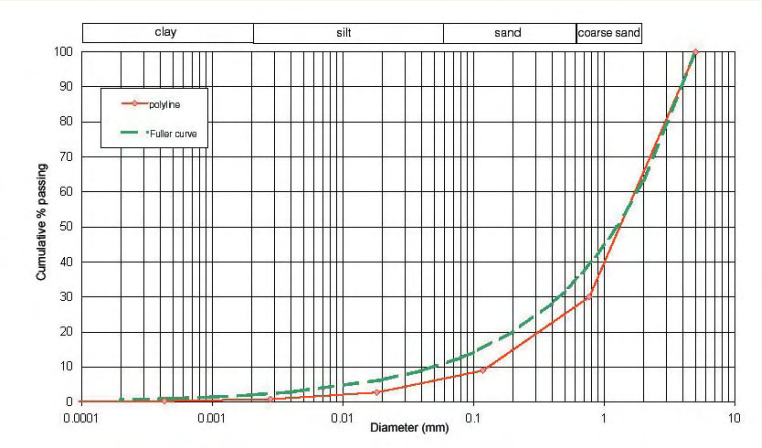

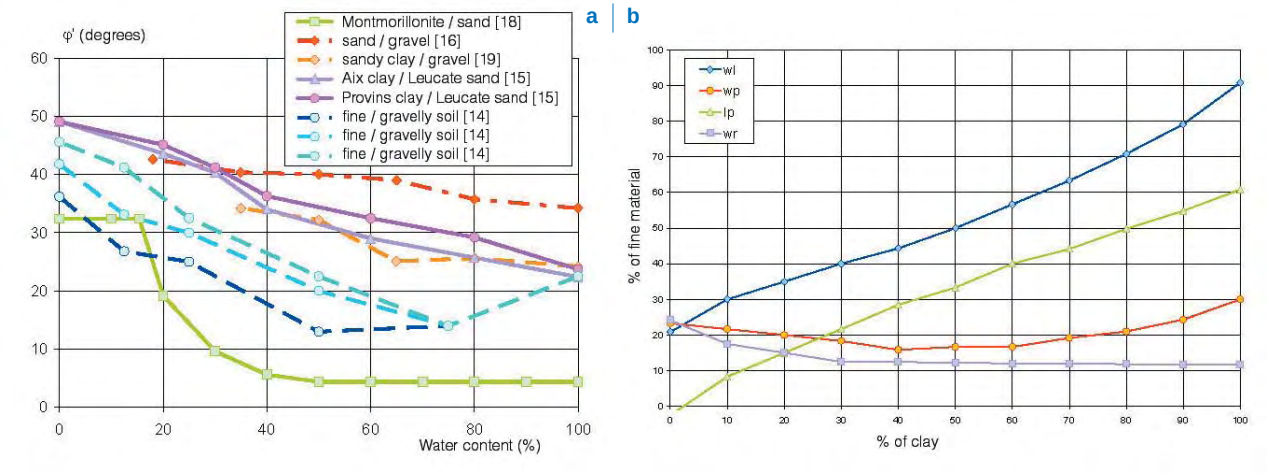

figure 6
- a: Variations in angle of friction with the percentage of fines
- b: Plasticity parameters with the sand content in Montmorillonite-type clay (extracted from **[18]***)*

The fine soil and coarse granular material mixes experience a maximum in their dry void index for a coarse grain percentage of approximately 60%, and this would apparently be due to the fact that as the percentage of coarse grains rises, the mortar itself is less well-compacted **[20]**. This poorer particle fit would explain the drop in shear strength observed on **Figure 6**. In subsequent research, this behavior has been theoretically confirmed **[21]**.

Evolution in the angle of friction with an increase in the fine fraction, as observed on **Figure 6a**, resembles very closely the relations previously proposed **[22, 23]**, which describe a sharp drop in the angle of friction with the plasticity index, which to a certain extent represents the influence of the fine fraction **(Fig. 6b)**.

Research was thus aimed at studying the influence of the proportion of granular fractions on mechanical parameters by carrying out consolidated-undrained triaxial testing. The specimen production procedure employed is the conventional one, yet extra special attention was paid to the knowledge of relative sample density.

The use of an instrument enabling local measurements of both axial and radial deformations has made it possible to obtain the modulus of deformation from measurements taken over the central part of the specimen, which is the zone where deformations are the most homogeneous, as well as volume variations.

The experimental protocol was designed in a way that allows differentiating the set of parameters governing the behavior of these heterogeneous soils in both shear and deformation. The role of several parameters has also been examined:

– the ratio between minimum and maximum diameters,
– the respective percentages of the various particle size fractions, and
– the shape of the particle size distribution curve.

A critical analysis of these tests will be presented. Results have been complemented by other behavioral measurements available in the bibliography **[11,12]**. The predictions of a two-component mix model inspired by the University of Cambridge model and based on the work of Cola and of Omine **[11,12]** will then be compared with experimental results.

PRESENTATION OF THE EXPERIMENTAL CAMPAIGN

Undrained tests on mixes composed of glass beads and Fontainebleau sand

Six mixes were prepared with a ratio of 30% fines and 70% coarse elements. An initial series was composed of 8-mm diameter beads mixed with sand, 1.5-mm beads and 3-mm beads. A second series contained 1.5-mm beads with beads sized 3 mm, 6 mm and 10 mm for the purpose of verifying the optimal ratio between particle grain sizes **[24]** **(Fig. 7a)**.

A total of five two-component mixes (8-mm and 1.5-mm beads (ratio ≈ 6.5)) with various percentages of 1.5-mm beads (20%, 30%, 40%, 50% and 70%) were produced in order to identify the proportion that corresponds to the best arrangement **(Fig. 7b)**.

Specimens have been generated directly in the triaxial apparatus with dimensions of 70 mm in height and 38 mm in diameter; they were then sheared at three distinct effective confining pressures σ'_3: 100 kPa, 200 kPa and 300 kPa, respectively, without introduction of any back pressure.

The pore-air pressure measurement has yielded a qualitative interpretation of the tests. **Figures 8a** and **8b** clearly show the simultaneous variation of both the deviator and pore pressure corresponding to the particle rearrangements.

figure 7
The particle size distribution curves of mixes

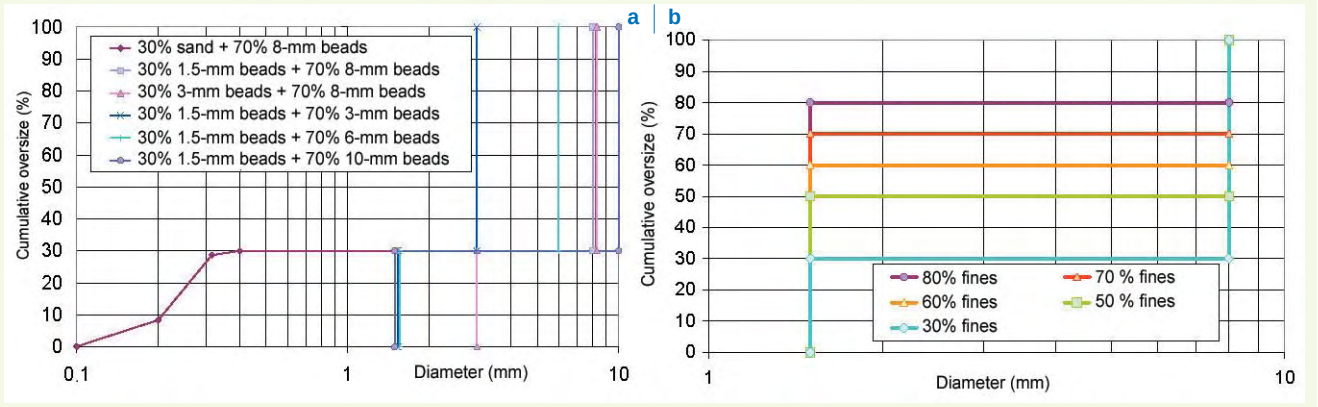

figure 8
Mix containing 70% 8-mm beads and 30% Fontainebleau sand
- a: q - ε_1 relations
- b: u_{air} - ε_1 relations

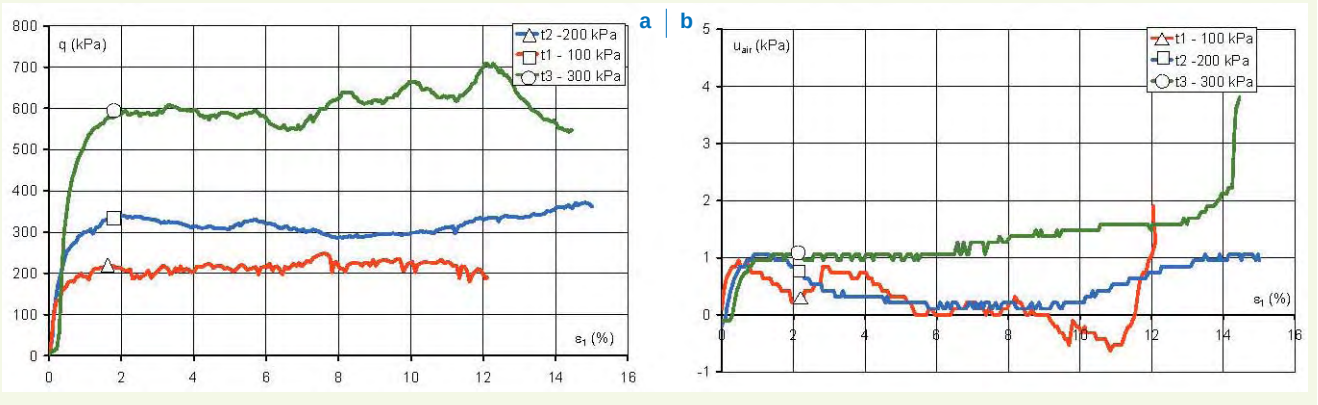

Undrained tests on mixes composed of Leucate sand and kaolinite

Five mixes containing sand and kaolinite, with kaolinite (C) percentages spanning 0%, 30%, 50%, 70% and 100%, were prepared **(Fig. 9)**. Each mix was developed using an optimal water content, as determined from the normal Proctor test, in order to maximize density **[25]**.

With each mix, three specimens 76 mm high and 38 mm in diameter were produced and then sheared using three distinct effective confining pressures σ'_3: 100 kPa, 200 kPa and 300 kPa, respectively, with a back pressure of 400 kPa.

For the pure sand mix (i.e. 0% kaolinite), it could be observed that the deviator rises to a peak before dropping rather abruptly towards a low asymptotic value, and the pore pressure climbs to a maximum and then also decreases rapidly. As for the undrained tests conducted on the sand, density winds up exerting a sizable influence on behavior. The void index obtained for the sand is relatively small (0.58), which causes an apparent excess consolidation **[26]**; little contraction therefore occurs at the beginning with dilatation afterwards **(Figs. 10a** and **10b)**. It is also observed that the resultant air pore pressure is much higher than that measured during tests conducted on glass beads due to a much lower permeability **(Figs. 8b** and **10b)**.

For the other mixes, observations during shear indicate an increase in air pore pressure u_{air} followed by a steady decrease once failure has been reached. The stress deviator increases continuously with strain, even at the failure point. Moreover, both the deviator and pore pressure associated with the mix drop with a rise in kaolinite (C) percentage **(Figs. 10a** and **10b)**. The mix thus proves to be stronger at a higher percentage of sand.

The curves obtained fit very clearly within the previously proposed typology **[27]**, which serves to qualify these tests as being of high quality.

figure 9
The particle size distribution curves of mixes

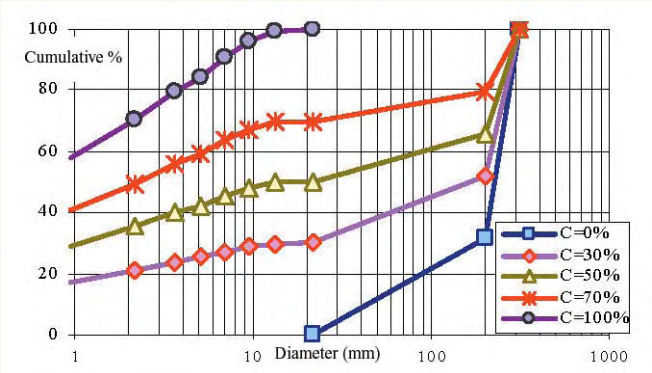

figure 10
- a: q - ε_1 relations of mixes at σ'_3 = 200 kPa
- b: u_{air} - ε_1 relations of mixes at σ'_3 = 200 kPa

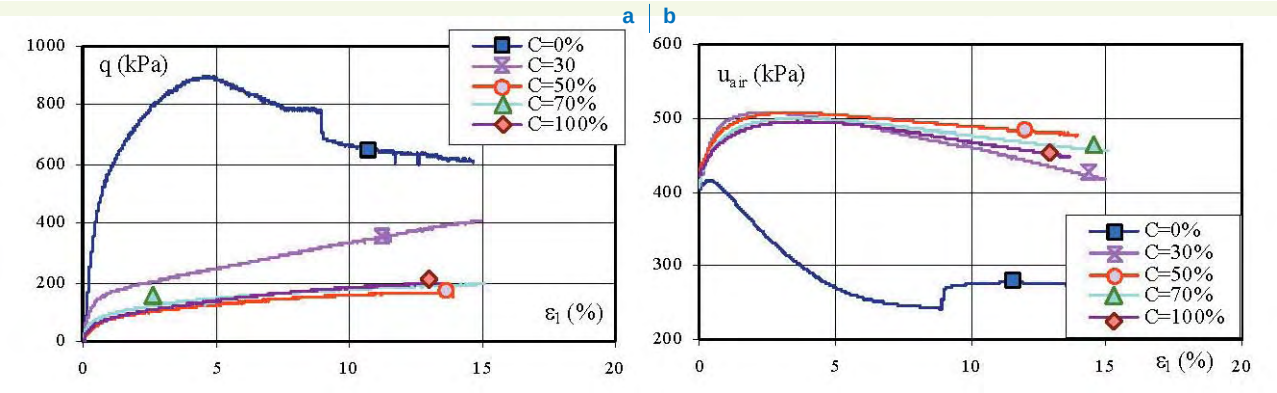

INFLUENCE OF THE d_{large} / d_{small} RATIO

The relative sizes of the coarse and fine particles constitutes an influential factor on the two-component mix by the interlocking of small particles within the voids lying between the larger particles. The tests conducted enable observing the same trend with a threshold situated at roughly d_{large} / d_{small} ≈ 6.5 **(Fig. 11a)**.

It would also appear that the angle of internal friction for a mix composed of 30% fines increases quickly when raising the large grain diameter-to-small diameter ratio, until reaching a value of approximately 7. Once this value has been exceeded, the angle of internal friction between the elements still increases, yet significantly less sharply **(Fig. 11b)**.

It can still be noted however that the curve shape is not very distinct, which may be due to the use of beads that limit this interlocking effect typically as a result of the grain faces.

figure 11
Variations in:
- a: void index with the ratio of diameters
- b: angle of friction with the ratio of diameters

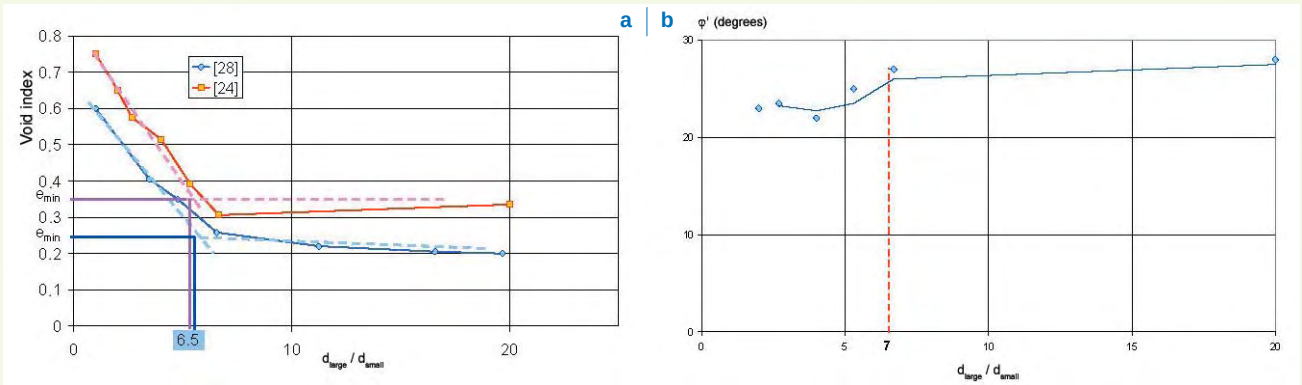

INFLUENCE OF THE PERCENTAGES OF LARGE AND SMALL GRAINS

For a two-component mix, when the percentage of fines (C) is 0%, the mix void index equals that of the coarse particles. As the fines percentage rises just a bit, these particles fit into the voids formed between the large grains, the void index falls, hits a minimum and then climbs **(Fig. 12)**. The minimum void index value (e_{min}) is reaches when the voids between the larger grains are completely filled by the fines **[5]**. The percentage corresponding with this threshold is denoted Cr **(Fig. 12)**.

When C < Cr, the fine fraction exerts little impact on mix behavior, as the mix is dominated by the coarse fraction. On the other hand, once the percentage C has attained a value of 70% to 80%, barely any interactions are taking place between the coarse particles, which get dispersed within a matrix

figure 12
Variation in void index with both the ratio of diameters and percentage of fines

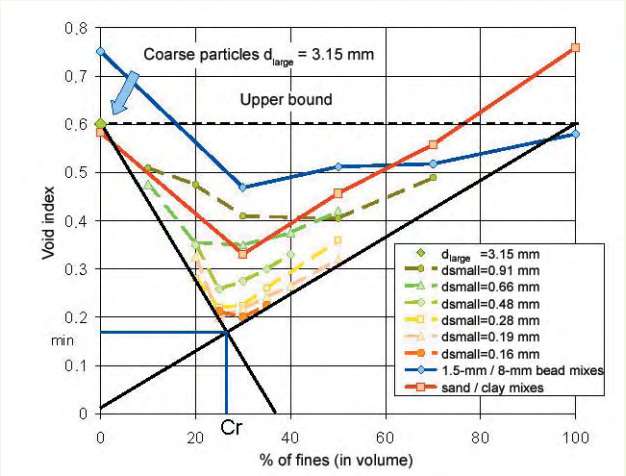

of fines: the mix behavior is then being dictated by the fines. It is often found that this threshold Cr lies on the order of 20% to 30% **(Fig. 12)**. At this threshold, density is maximized, which induces higher material strength.

The angles of friction measured do not change significantly prior to reaching the threshold (20%-30%) and then drop as the fines percentage increases **(Fig. 13)**.

Nonetheless, the shape of the curves for the beads-sand mix **(Fig. 13, [24])** is not as distinct as those derived by other authors; this may be caused by the use of spherical shapes that serve to attenuate the overlapping effect due to the natural grain faces, as this effect must be proportional to the grain size.

As regards the shear modulus **[11, 25]** or secant modulus calculated at 50% of the maximum shear strength (E_{50}, **[12]**), an increase can also be observed during the decrease in fines percentage **(Fig. 14)**.

figure 13
Variations in angle of friction with the percentage of fines obtained by various authors

figure 14
Variations in shear modulus G and secant modulus E_{50} with the percentage of fines

13 14

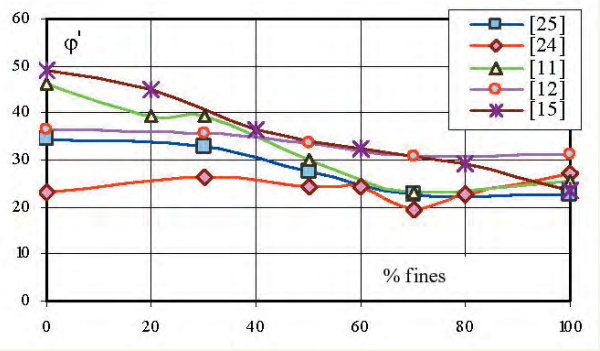

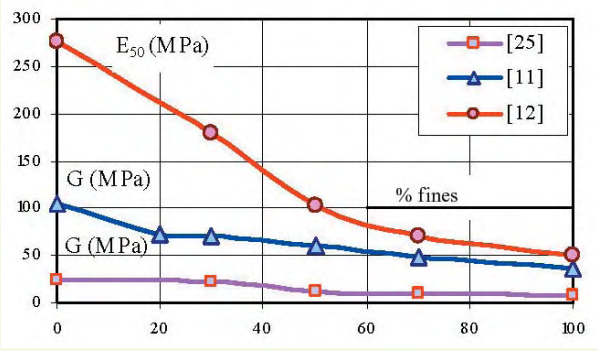

INFLUENCE OF THE PARTICLE SIZE DISTRIBUTION CURVE SHAPE

The results derived serve to better understand the behavior of the natural coarse soils observed during the previous experimental campaigns **[29,30]**.

Since the use of parameters like d_{10} (grain diameter for a 10% sieve passing rate) and $C_U = d_{60}/d_{10}$ does not generate information on the shape of the material's particle size distribution curve, Burminster **[31]** proposed classifying particle size distribution curves into five categories that can then be broken down into subcategories by combination of the five letters D, S, L, C and E **(Fig. 15)**. The coefficient Cb describes the average slope of the particle size distribution curve (d_{max} and d_{min} are the minimum and maximum values of the linear regression). Subsequently, Burminster **[31]** and Holtz **[17]** derived a clear relationship between the parameter Cb and the curve shape. The mixes of fine soils with coarse granular materials (case of the "D" curve) provide an exception to this rule. This stepwise shape of curve D is due to the various mixes: case of alluvial gravel displaying "sand mounds".

The analysis of shear strength results suggests proposing the following interpretation: for those materials whose particle size distribution curve is hollow, i.e. concave upward, display a higher optimal density and thus a more efficient overlap of particles **(Fig. 15)**. Consequently, higher shear strength can be observed for these materials **(Figs. 16** and **6a)**.

Figure 17 shows that parameters C_U and $C_C = d_{30}^2/d_{10}.d_{60}$, which were classically adopted to characterize the particle size distribution curves, do not yield information of any practical utility. An increase in these parameters is nonetheless apparent when approaching the optimal void-filling point.

figure 15
Variation in density with the particle size distribution curve shape (extracted from **[31]***)*

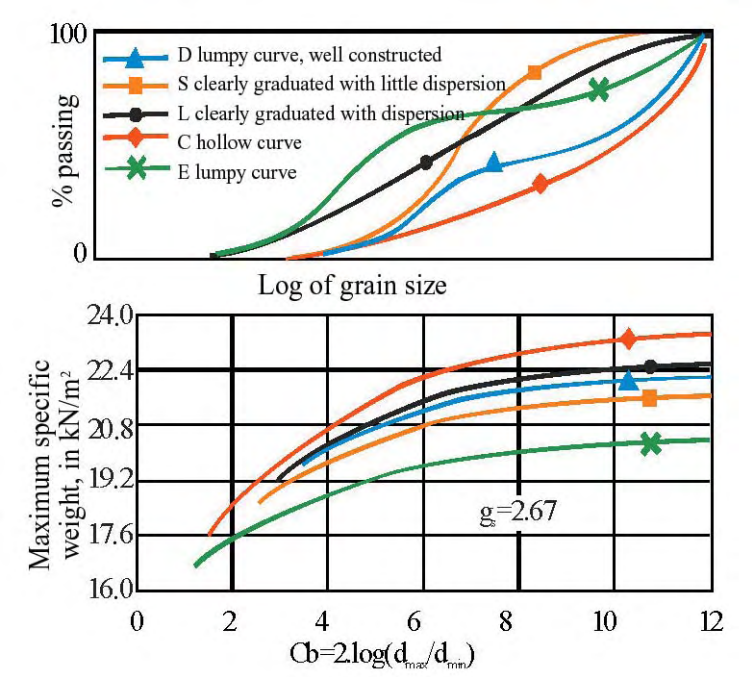

figure 16
Variation in density with the particle size distribution curve shape

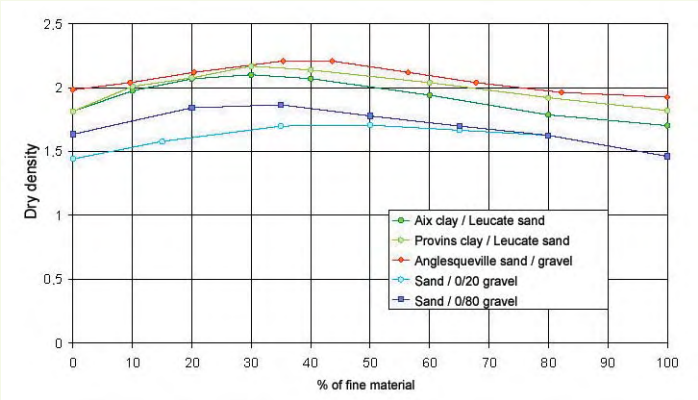

figure 17
Variation in parameters CC and CU with the percentage of fines

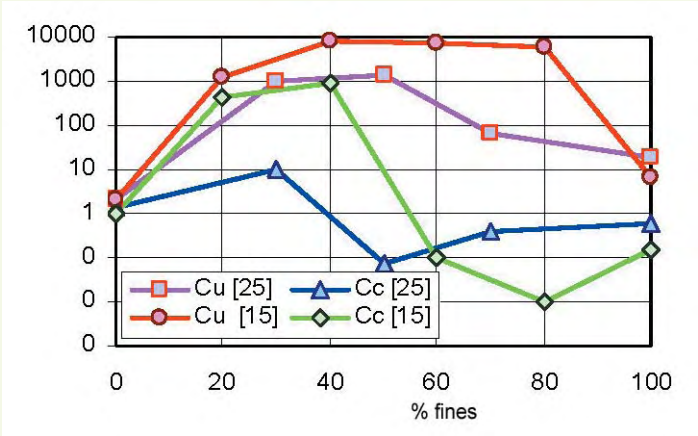

The coefficient Cb, calculated for the soils under study, evolves in accordance with what had been proposed by Burminster: dry density increases with the coefficient Cb **(Figs. 15** and **18)**. Here once again, however, a less distinct evolution has been noticed for natural granular materials than for the artificial mixes, with the mixes featuring Cb values greater than the original materials.

figure 18
Variation in density with the particle size distribution curve shape

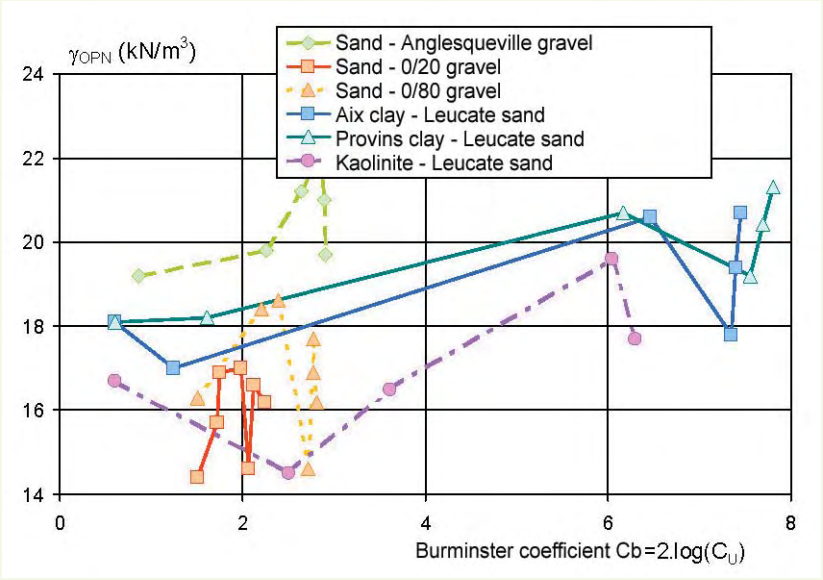

MODELING OF MIX RHEOLOGY

The focus is primarily placed on the approach known under the name "mix theory", which leads to models of the continuous medium type as well as to applications using the finite element method. The two-component mix model described below has been drawn from the research work of Cola and of Omine **[11,12]**; this model is of an elastoplastic type and only requires the determination of a small number of parameters. The model has been built based on the critical state concept, with rupture obeying a Mohr-Coulomb criterion. This type of model offers the advantage of merely requiring a test to be carried out on a single material fraction, as opposed to other more sophisticated models **[32]**. This amounts to a considerable advantage whenever the particle size distribution is not compatible with the materiel available within the limitations of the study.

The soils or heterogeneous mixes can be diagrammed just like the two-component mixes, in which a coarse fraction (CF), containing granular materials, is interacting with the fine fraction or matrix (FF), with the matrix being impregnated by liquid and/or gaseous phases **[33]**. Their overall properties depend on the particle size distribution and shape of the coarse particles, as well as on the fine fraction mineralogy, water content and especially the CF and FF percentages.

Definition of variables

In the saturated two-component mixes, i.e. the CF and FF components, the proportion of fine materials C is defined as the ratio of FF mass to total solid mass. Since the densities of constituents are typically very close to one another, the quantity C can also be expressed as a volume ratio.

Let V_w, V_C, and V_G represent the volumes of water, FF and CF respectively, and e the void index of the mix, then the two other void indices, i.e. those of the coarse fraction and the matrix e_G and e_C, may be defined by Mitchell's equation **[33]**:

$$e_G = \frac{V_W + V_C}{V_G} = \frac{100e + C}{100 - C} \;;\; e_C = \frac{V_W}{V_C} = \frac{100e}{C} \qquad (3)$$

The two values of e (one a function of e_G and the other of e_C) correspond to the LT and TS lines shown in **Figure 1**; it thus becomes necessary to take the greater of these two values in order to generate the envelope curve.

At a high value of C, the CF grains are not in contact with one another and the forces split between the two fractions according to the relative stiffness of components. As C decreases, the possibility that two or more grains make contact increases quickly: when such contact occurs, the grains form a stiffer skeleton and, on the inside, the entrapped FF are not able to deform or support the force increments, thereby becoming a part of the skeleton. When C = Cr, all grains lie in contact with one another and the soil behaves like a granular material. As suggested by Omine *et al.* **[12]**, it is convenient to distinguish two FF and CF parts: one composing the skeleton (V'_w, V'_C and V'_G), and the other the matrix (V''_w, V''_C and V''_G). It is to be noted that V''_G represents the volume of grains completely immersed in the matrix. In conformance with this hypothesis, the fractions of both matrix volume f_C and skeleton volume R are defined as follows:

$$f_C = \frac{V''_W + V''_C}{V} \;;\; R = \frac{V'_W + V'_C + V'_G}{V} \tag{4}$$

Omine **[12]** proposed a relation that expresses the fraction of volume f_C:

$$f_C = 1 - \left[1 + (1 + e_{co})\left(\frac{C}{100 - C} - \frac{C_r}{100 - C_r}\right)\right]^{-1} \tag{5}$$

where e_{co} is the void index of the matrix at C = 100%. On the basis of a probability analysis of the assemblies of grains in contact with one another, Omine **[12]** suggested that *R* could be correlated with parameter f_C by means of the following simple relationship:

$$R = (1 - f_C)^2 \tag{6}$$

It is noted that at C = 100%, the volume fractions become $f_C = 1$ and $R = 0$, while when C = Cr, the presence of the matrix disappears and the values $f_C = 0$ and $R = 1$ are obtained.

Model expression

In order to evaluate the distribution of forces in the two soil components and properties of a mix, Omine *et al.* **[12]** introduced a force distribution parameter *b*, defined by:

$$dq_C = b\,dq_G \;;\; dp'_C = b\,dp'_G \tag{7}$$

where d*q* and d*p*' are the deviatoric and average effective stress increments, with the indices G and C referring to the skeleton and matrix, respectively.

The parameter *b* represents the ratio between the stress increments. If the two fractions are isotropic and elastic, *b* is a constant and the quantities *q* and *p'* may be substituted for the increments d*q* and d*p*' in Equation (7). In all other situations, *b* depends on both the load conditions and the unique specific volume.

To determine *b*, it is assumed in the present context that stress increments are being absorbed with an equal distribution of internal work between the two fractions. Moreover, an elastoplastic model of the modified Cam-Clay type **[34,35]** is used as the constitutive model for both fractions.

Elastic conditions

In isotropic elastic compression, the specific volume (or void index) $v = 1 + e$ is linearly correlated with the Neperian logarithm of the average stress *p'*. If κ is the slope of the *e*-ln *p*' curve, then by combining the relations between elastic volumetric deformation and the internal work of the skeleton and matrix, the following is obtained:

$$\frac{\kappa}{v} = R\frac{\kappa_G}{v_G} + f_C\frac{\kappa_C}{v_C} \tag{8}$$

In simple shear within the elastic zone, the expression for shear stress increments and internal work for both fractions enables writing the global shear modulus G and parameter b as follows:

$$b = \left(G_G / G_C\right)^{0,5} \text{ et } G = \left(R.b + 1 - R\right) \Big/ \left(\frac{R.b}{G_G} + \frac{f_C}{G_C}\right). \quad (9)$$

where G_G and G_C represent the shear modulus of the skeleton and matrix, respectively.

Plastic conditions

Within the modified Cam-Clay model, the load surface and plastic deformations ε_p^p and ε_q^p for a general stress increment exceeding the elastic zone are:

$$p' = \frac{M^2}{M^2 - \eta^2} p'_o \; ; \; d\varepsilon_p^p = \frac{\lambda - \kappa}{v} \frac{dp'_o}{p'_o} \; ; \; d\varepsilon_q^p = \frac{2\eta}{M^2 - \eta^2} d\varepsilon_p^p \quad (10)$$

where M, λ and κ are the model parameters, and $\eta = q/p$ and p'_o describe the common size of the load surface ellipse. It is assumed that the two components and mix occupy an equivalent state with respect to the critical state, with the result being that for a hydrostatic load increment, the quantity λ/v is written:

$$\frac{\lambda}{v} = R\frac{\lambda_G}{v_G} + f_C \frac{\lambda_C}{v_C} \quad (11)$$

In expressing the shear stress of the mix at the critical state, the slope M of the critical state boundary can be written as follows:

$$M = \left(R.b + f_C\right) \Big/ \left(\frac{R.b}{M_G} + \frac{f_C}{M_C}\right) \quad (12)$$

The parameters determined previously are now introduced into the modified Cam-Clay model in order to model the undrained behavior of the mixes.

Experimental validation

Two experimental studies have been conducted, the first in Japan by Omine, for the purpose of validating the "mix" part of the model and the other in Italy to validate the "Cam-Clay" part, without necessarily focusing on the stress-strain relations or stress paths **[11,12]**. An identical study was undertaken in 2004 at the LCPC laboratory in the aim of validating these last aspects.

The mix is produced using Toyoura sand ($d_{50} = 0.17$ mm, $C_U = d_{100}/d_0 = 5.86$ **[11]**, $e_{max} = 0.988$, $e_{min} = 0.616$ and $\gamma_{sG} = 26.5$ kN/m^3) and a kaolinite that were mixed at a water content value lying between 1.5 and 1.8 times the liquidity limit, with kaolinite percentages C of 0%, 30%, 50%, 70% and 100%.

The undrained triaxial test specimens were cut from blocks consolidated beforehand in a mold. The granular soils were set into place either by pluviation or by scooping. The triaxial specimens were consolidated at a pressure of 98 kPa. Lastly, undrained shear was introduced at a deformation speed of 0.07%/min.

For the tests conducted by Cola **[11]**, the mix was produced from limestone gravel ($d_{50} = 4.87$ mm, $C_U = d_{60}/d_{10} = 1.48$ and $\gamma s_G = 27.0$ kN/m^3) and a kaolinite ($d_{50} = 1.3$ mm, CF = 58, $w_L = 59\%$, $w_P = 39\%$ and $\gamma_{sF} = 26.3$ kN/m^3), which were mixed at a water content level of 1.5 to 1.8 times the liquidity limit and then consolidated with kaolinite percentages (C) of 0%, 20%, 30%, 50%, 70% and 100%.

Figures 19a through **19e** compare theoretical results with the values of variables either measured or deduced from the interpretation of experimental results. **Figure 19a** depicts results in terms of void

index. Odometric tests conducted on specimens 8 cm in diameter and 5 cm thick led to comparing **Figures 19b** and **19c** (i.e. variation in the κ/v and λ/v parameters). The deformation parameter G and rupture parameter M represented on **Figures 19d** and **19e** were deduced from the triaxial tests.

The theoretical behavior calculated using the mix model **(Figs. 19)** correlates well with observations made during experiments performed on the variations of *e, M,* E_{oed} derived by Omine *et al.* **[12]** and Cola **[11]**. An identical behavior was partially observed by Dupla *et al.* **[36]** on mixes containing glass beads and Fontainebleau sand.

figure 19
Validation of the mix model by means of the Omine and Cola tests **[11-12]:**
- a: void index
- b: κ/v
- c: λ/v
- d: M
- e: G

It seems however that for a percentage of fines (i.e. a value of C) of less than 33%, material behavior is dictated by the granular skeleton. Due to this fact, the influence of void index is seen to be significant. Despite the application of standardized procedures, the pure granular material could not be applied to a high enough void index, which incited using the values obtained for C = 20% as

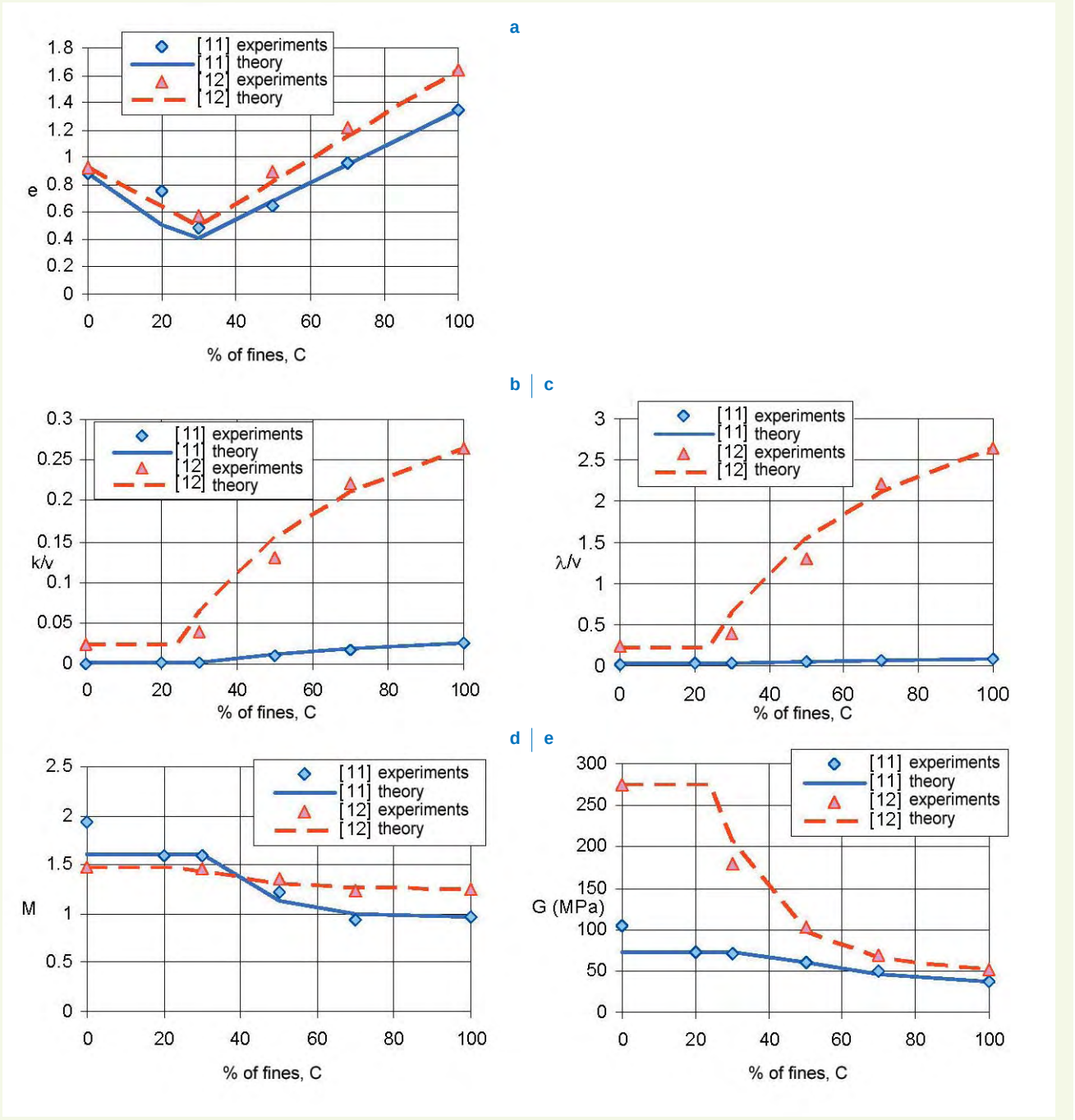

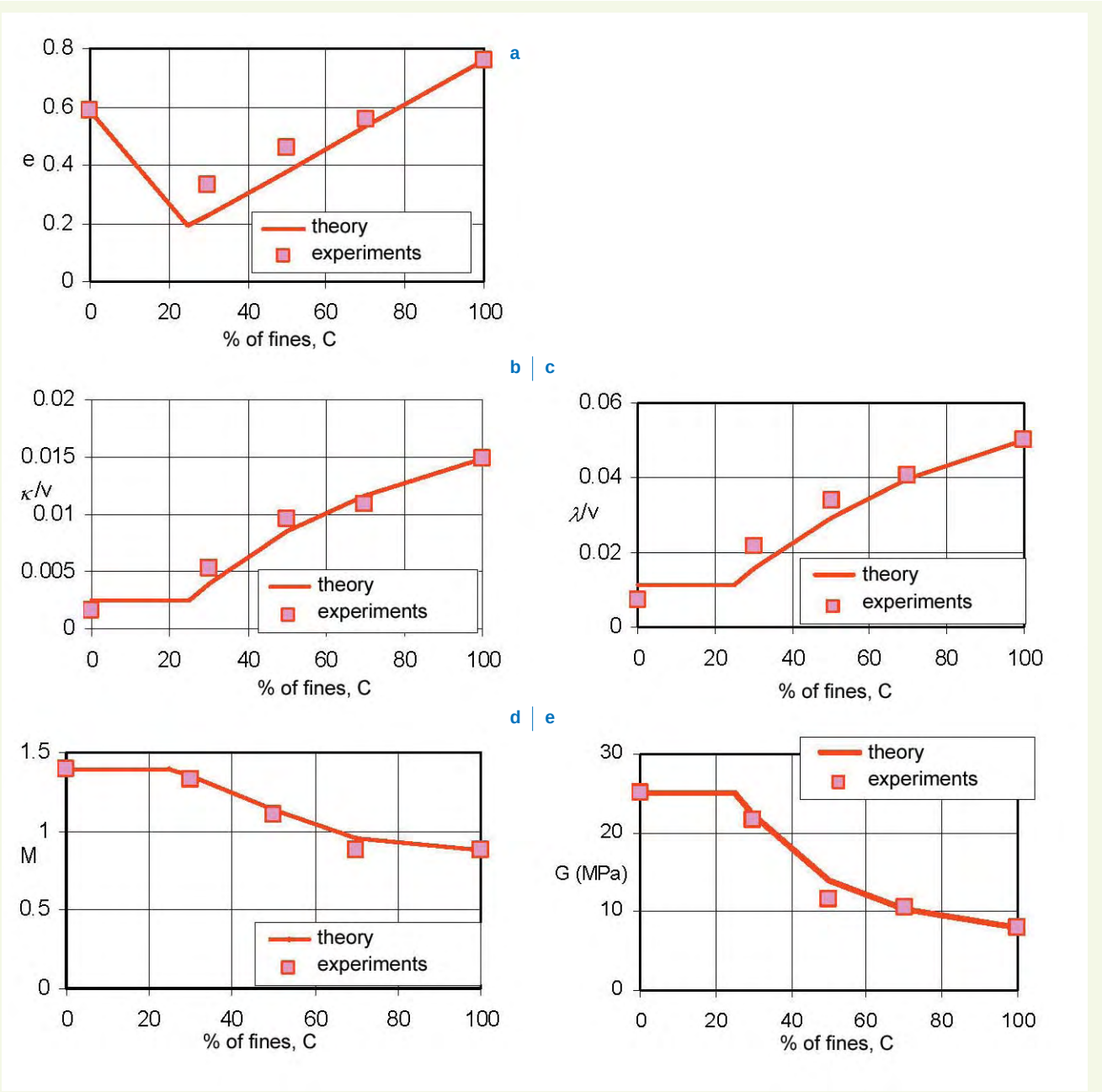

figure 20
Comparison of mix parameters between theory and experimentation:
- a: void index
- b: κ
- c: λ
- d: M
- e: G

behavioral limitations. From the tests carried out in LCPC's soil mechanics laboratory, the strong correlation between theoretical simulation and experimental findings could also be determined **(see Fig. 20)**.

Mix behavior in the u–ε_1 and q–ε_1 planes

In the *(q–ε$_1$)* and *(u–ε$_1$)* planes **(Figs. 21** to **24)**, a strong level of agreement between the theoretical and experimental curves can be observed. This agreement is better for the clayey mixes than for the sandy ones. The values of *u* and *q*, as measured in the laboratory, are always less than those derived theoretically, which could be explained in part by observing the void index diagram obtained using the theoretical model and the set of experimental results **(Fig. 20a)**. Like with Cola's tests, the sand exhibits an overly low void index **[11]**. If in future experiments, specimens can be prepared with a void index that matches the one proposed by the theoretical model, it will be possible to generate a good level of correlation.

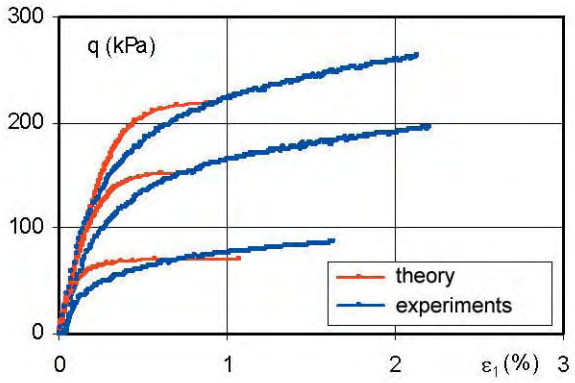

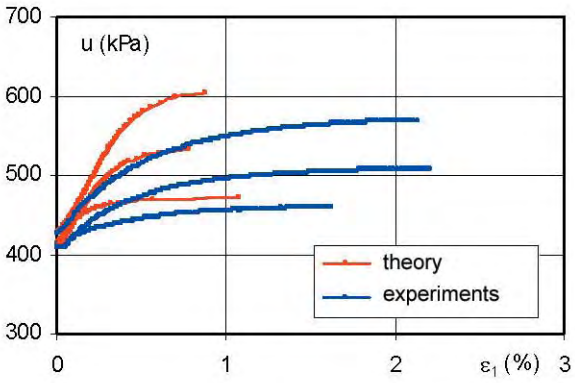

figure 21

(q - ε_1) and (u - ε_1) relations of the mix for 30% kaolinite

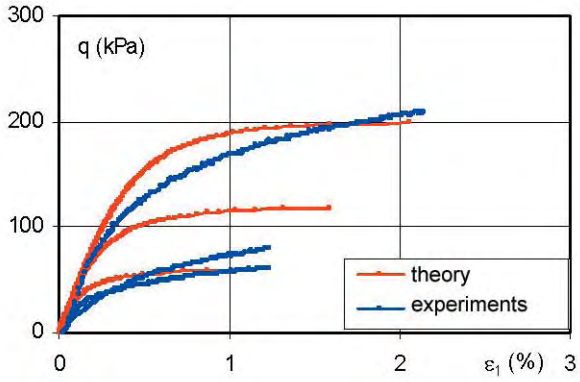

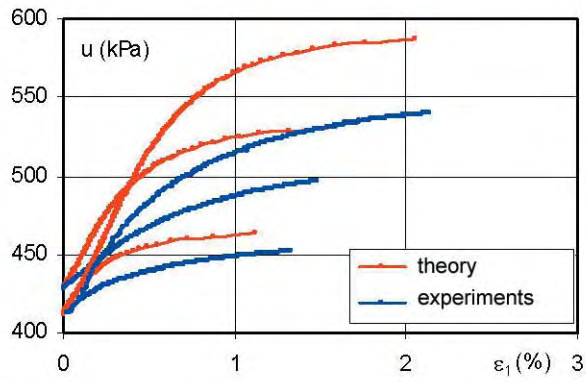

figure 22

(q - ε_1) and (u - ε_1) relations of the mix for 50% kaolinite

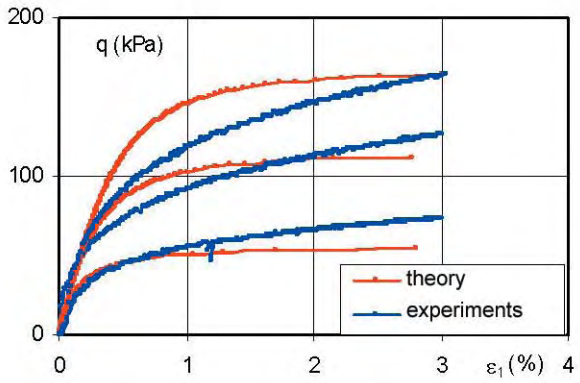

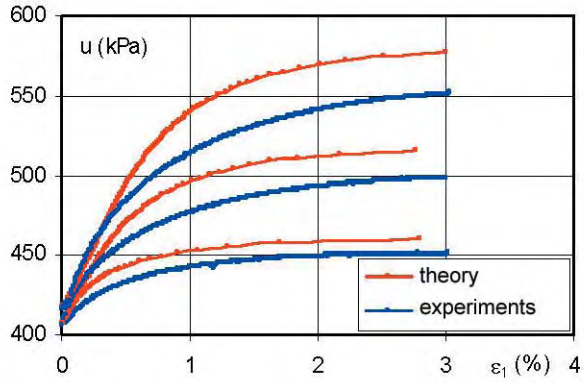

figure 23

(q - ε_1) and (u - ε_1) relations of the mix for 70% kaolinite

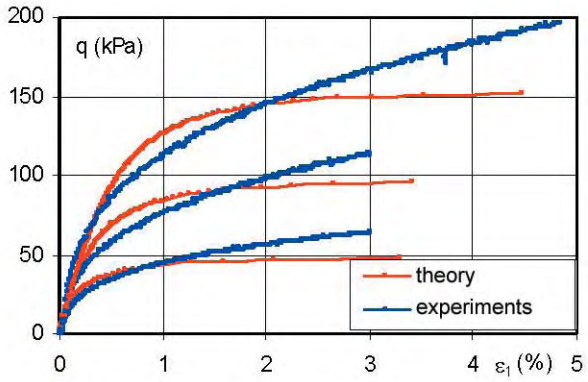

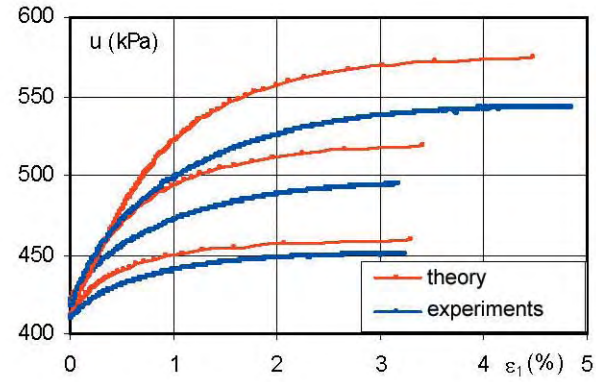

figure 24

(q - ε_1) et (u - ε_1) relations of the mix for 100% kaolinite

Mix behavior in the p'- q plane

figure 25
Comparison in the (p'- q) plane between theory and experimentation for various kaolinite percentages:
- a: 30%
- b: 50%
- c: 70%
- d: 100%

On **Figure 25**, stress paths were compared in the (*p'– q)* plane proposed by the model with those followed by specimens during testing. For the mixes at 50%, 70% and 100%, a good level of overlap exists between theory and experiment; as a case in point, the curves in this figure are nearly superimposed on one another. For the mix at 30%, it was determined that the average effective stresses from the experimental campaign are indeed higher than those predicted by the theoretical model, perhaps because of the somewhat greater offset in the void index with respect to those of the other mixes (see **Fig. 20a)**.

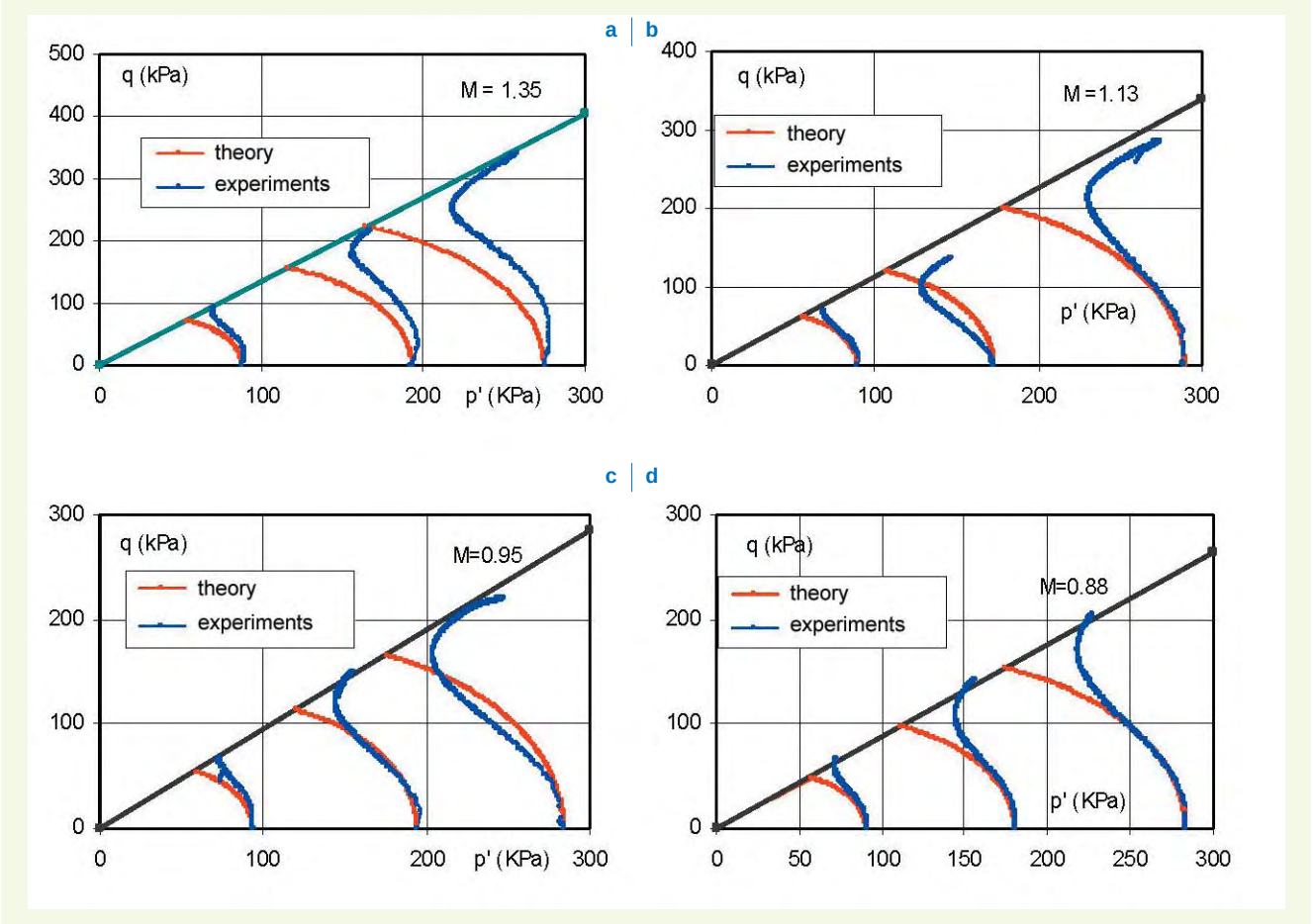

VALIDATION ON CRIQUEBEUF-SUR-SEINE SOIL

In order to validate the mix model on a natural soil, an experimental program was conducted at the road testing center in Rouen (Normandy) using a large-sized triaxial device designed for tests on reconstituted soil specimens 30 cm in diameter and 60 cm high **[2,37]**. The experimental program consists of tests on a reference soil, which is alluvial gravel from the small town of Criquebeuf with a 0/80 mm particle size fraction **[2]**. This gravel was separated into a 0/25 mm fraction, composed of the fine fraction that can be tested by a conventional triaxial device 150 mm in diameter, and a 25/50 fraction representing the coarse particles.

The experimental approach calls for conducting CU + u tests at pressures of 100, 200 and 300 kPa on reconstituted specimens at 95% of the OPN level by varying the coarse fraction proportion with respect to the fine fraction. These tests were carried out using various 0/25 mm fine fraction percentages C (0%, 30%, 50%, 70% and 100%). The undrained triaxial test specimens were reconstituted by means of vibratory compression **[2]**. The triaxial specimens were consolidated at a pressure of 100 kPa. Lastly, the undrained shear was introduced at a deformation speed equal to 7.10^{-2}%/min **(Fig. 26)**.

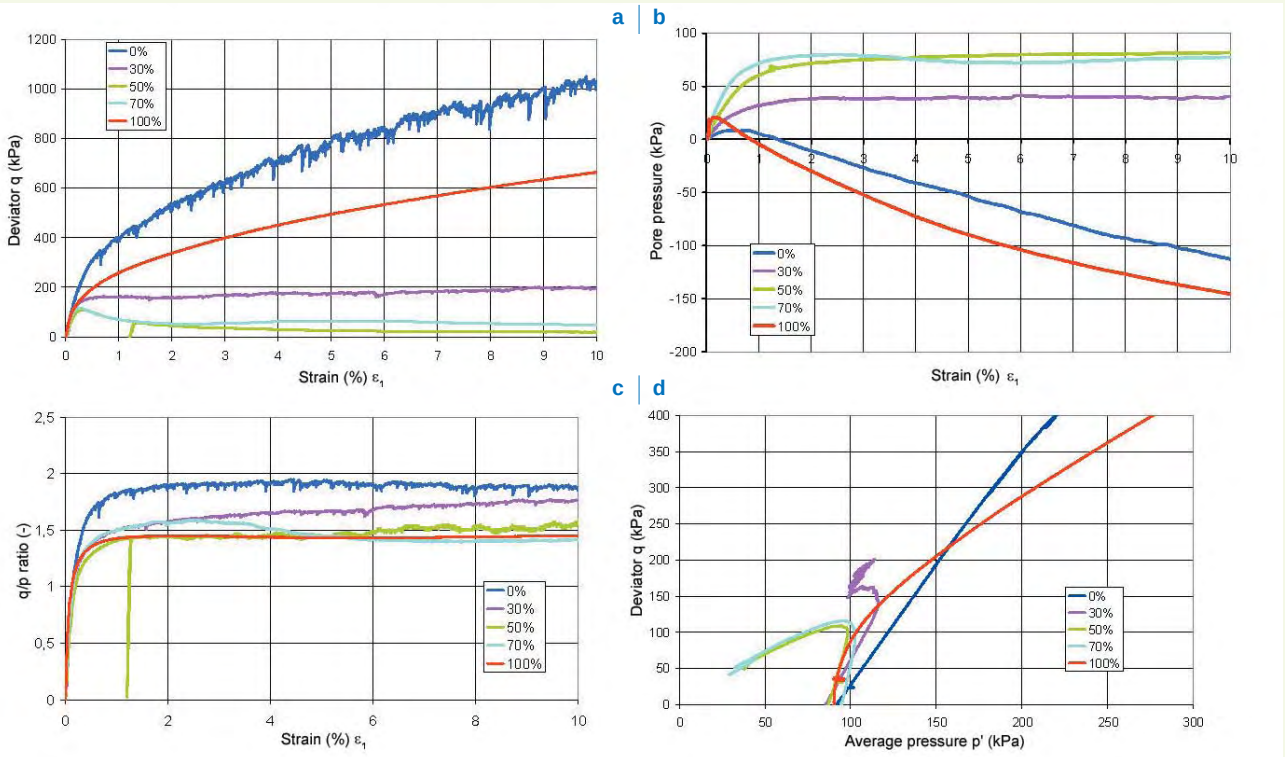

figure 26
Results from triaxial tests conducted on soil from Criquebeuf at a 100-kPa confinement stress:
- a: deviator vs. deformation
- b: pore pressure vs. deformation
- c: primary stress ratio vs. deformation
- d: deviator vs. average pressure (extracted from **[37]***)*

The results obtained on the Criquebeuf gravel have been superimposed on the graphs shown in **Figure 27** with the variations in e, M and G as predicted by the mix model. The tangent shear modulus and secant shear modulus were also indicated and determined to equal 0.05% and 0.3% of deformation, respectively. The odometric characteristics were deduced from the consolidation phase on a series of tests with a 500-mm square direct shear box conducted in parallel.

It is easily observed that for a fines percentage of below 30%, material behavior is dictated by the granular skeleton. Since the particle size distributions proved to be less sharply contrasted than for the "model" materials however, the trends noted on **Figure 27** are not as distinct as on **Figures 19** and **20**; this aspect had already been highlighted on **Figure 6a**. The differences observed may be due to the small difference existing between the average diameters of the two fractions 0/25 mm and 25/50 mm.

As a result of the more highly frictional nature of the fine fraction, the moduli values have been overestimated for the 30% and 50% mixes. The high modulus value obtained for the 0/25 mm fine fraction (100% fine fraction on **Figure 27c**) undoubtedly stems from over-compaction. This series has in fact served to establish the compaction protocol, which nonetheless has no impact on the slope of the critical state straight line.

It would thus seem plausible to predict the behavior of a natural coarse soil, for which only a fine fraction obtained by means of clipping can be laboratory tested. This course of action will be proposed in the following section on an experimental protocol drawn from the research work conducted by the French Public Works Ministry's technical network.

DISCUSSION

The application example concerns the rockslides on the A43 motorway studied in the laboratory by Shirdam **[38]**. According to the particle size distribution analysis both *in situ* and in the laboratory, these 0/250 materials contain 35% fines of a diameter less than 40 mm and have undergone extensive laboratory testing by the regional Ponts et Chaussées laboratory based in Lyon. Furthermore,

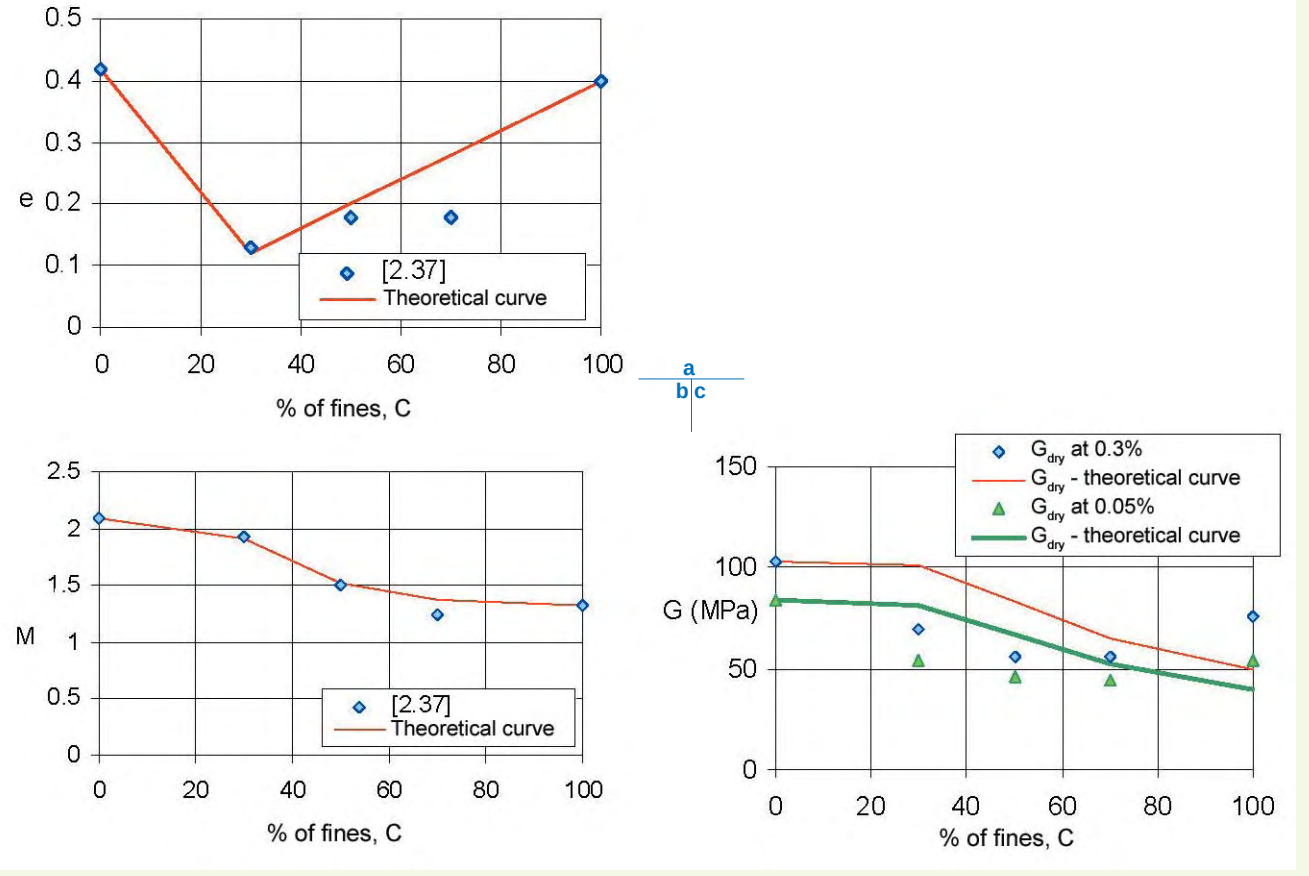

figure 27
Comparison of mix parameters between theory and experimentation:
- a: void index
- b: M
- c: G

these rockslides display a particle size distribution curve with a concavity that remains devoid of any bumps near a "C" curve defined by Burminster or one of the Fuller curves (C_U = 1,000 to 678 and C_C = 0.3 to 2,7, γ_h = 23.4 and γ_d = 22.5 kN/m^3) **(Fig. 28a)**. The 0/40 fine fraction composed of angular limestone grains was created by clipping and has been tested using the 600-mm diameter round shear box. The angle of friction was evaluated at 39 degrees and the cohesion measured to be 68 kPa. The angle of friction of the 0/250 natural material has been deduced from the failure analysis of the experimental embankment described by Shirdam, which yields an average value of 39-41 degrees and an *in situ* cohesion estimated at 25 kPa **[38]** **(Fig. 28b)**. Estimation of the *in situ* angle of friction by means of correlation leads to an average value of 45 degrees.

Based on shear test consolidation phase, the compressibility parameters Cs = 0.0066 and Cc = 0.13 may be estimated in order to obtain the parameters $\kappa = 0.003$ and $\lambda = 0.056$ required for model input. The pressuremeter modulus varies from 50 to 175 MPa at depths of between 6 and 10 m.

figure 28
- a: Particle size distribution curve for rockslides on the A43 motorway
- b: failure experiments on an embankment (extracted from **[38]***)*

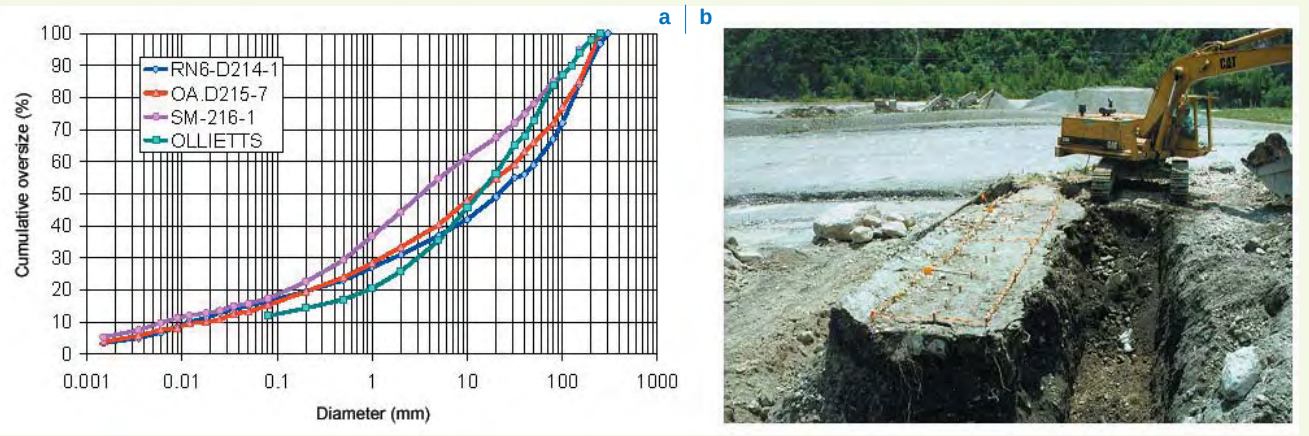

If excessively high values were to be eliminated (these are most likely due to tests conducted on blocks), a pressuremeter modulus of near 50 MPa would be obtained; this finding agrees with the odometric modulus evaluated at 16 MPa. The shear modulus might thus equal 25 MPa.

Lastly, in **Table 1**, mechanical parameters will be compared for:

– the 40/250 fraction, which has only been partially tested and for which parameters are estimated through the use of correlations;
– the 0/40 fraction, which has undergone in-depth laboratory testing; and
– the 0/250 natural material whose parameters are estimated by the mix model, *in situ* testing and the inverse failure analysis of an embankment.

Model predictions seem at first glance to provide reasonable estimations of the parameters required for computing a structure **(Fig. 29)**.

tableau 1
Parameters measured and predicted for the A43 rockslide

Parameter		e	λ	κ	G (MPa)	φ (deg.)/M
40/250 fraction		0.65	0.012	0.0028	75	47-49/1.93-2
		Abacus **[8]**	Cs = Cc/4	Correlations **[8]**	Correlations **[3]**	Correlations **[38]**
0/40 mm fraction		0.325	0.056	0.003	3.92	39/1.59
		Shear box **[38]**	Shear box **[38]**	Shear box **[38]**	Shear box **[38]**	Shear box **[38]**
Natural soil: 30% of 0/40 and 70% of 40/250	Mix model	0.15	0.01	0.0028	75	47/1.97
	Measure-ment on the natural soil **[38]**	0.24	-	-	25 to 87	42-45/1.78
		Calculated computed on the basis of densities measured *in situ*	-	-	Pressurem-eter	Pressurem-eter and embankment failure

CONCLUSION

Following a recall of the factors influencing the behavior of a heterogeneous, coarse soil, an approach based on mix behavior was presented herein. This approach has led to an elastoplastic model shaped around the concept of critical state, according to which rupture obeys a Mohr-Coulomb criterion.

In order to validate practical model applications, an experimental study has been undertaken and has included a series of triaxial tests on specimens reconstituted with beads, sand and kaolinite.

For mixes featuring two particle sizes, a ratio of either greater than or equal to 6.5 (between the largest and smallest diameters) allows minimizing the volume of voids and reaching a near-maximum angle of internal friction. It has been confirmed that a mix containing 30% fines and 70% coarse particles guarantees an optimal arrangement; moreover, it has been observed that shear strength is held at a maximum, which is not the case for the other mix proportions.

It thus appears that as the void index within the specimen lowers, both the mechanical behavior and shear strength of the mix are improved. The quantity of fines and hence the shape of the particle size distribution curve however serve to regulate the magnitude of the shear strength contribution.

An initial validation of the model proposed by Omine **[12]** and Cola **[11]** was performed on Fontainebleau sand-kaolinite mixes, followed by experiments carried out on the alluvial gravel from Criquebeuf-sur-Seine, have enabled confirming the potential applicability to actual materials.

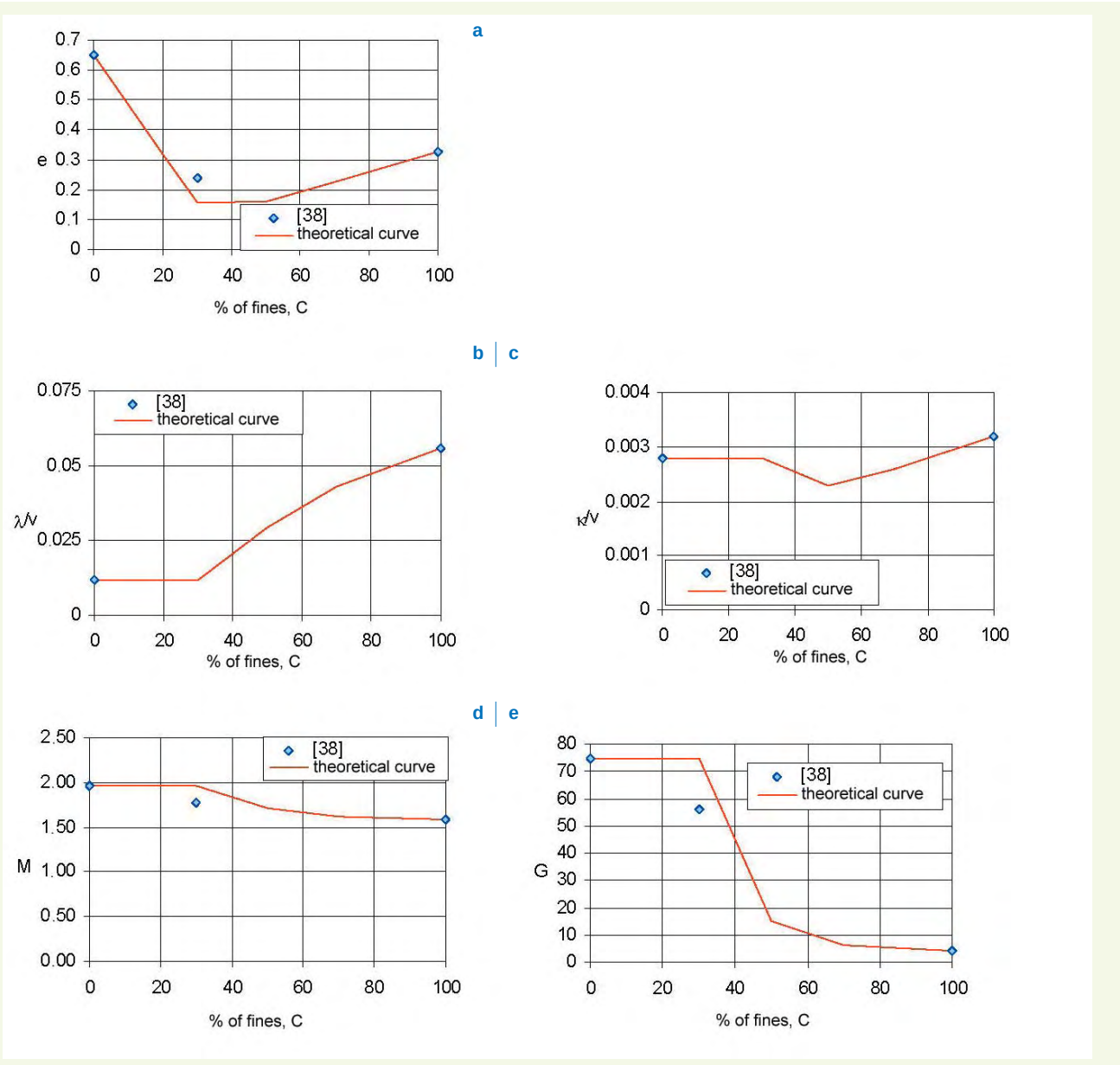

figure 29

Comparison of mix parameters between theory and experimentation for various fines percentages:
- a: void index
- b: κ
- c: λ
- d: M
- e: G

The validation on actual soil has made it possible to point out the potential use of this model within a practical context. The tool proposed by Omine **[12]** and Cola **[11]** thus seems to provide a relevant means of predicting the behavior of coarse materials within a modeling perspective.

ACKNOWLEDGMENTS

The authors would like to thank Mr. Jean-Louis Tacita (LCPC) as well as Ms. Myriam Nahum (with the Université Paris VI) for their valuable assistance during the experimental work discussed herein.

REFERENCES

1 **LCPC-Sétra**, *Guide pour les terrassements routiers*, **1992**, volumes **1** et **2**, 98 pages.

2 **Reiffsteck Ph.**, **Arbaut J.**, **Sagnard N.**, **Khay M.**, **Subrin D.**, **Chapeau C.**, **Levacher D.**, Mesure en laboratoire du comportement mécanique des sols hétérogènes, *Bulletin des laboratoires des ponts et chaussées*, **2007**, **268-269**, pp.

3 **Nedjat N.**, **Fry J.-J.**, *Une banque de donnée pour le calcul de barrage*, **1992**, RFG 60, pp. 71-81.

4 **Kézdi Á.**, **Réthàti L.**, *Handbook of soil mechanics*, Elsevier, **1986**.

5 **Lade P.V.**, **Liggio C.D.**, **Yamamuro J.A.**, *Effects of non-plastic fines on minimum and maximum void ratio of sand*, **1998**, GTJODJ 21 (4), pp. 336-347.

6 **Vallejo L.E.**, Interpretation of the limits in shear strength in binary granular mixtures, *Canadian geotechnical journal,* **2001**, **38**, pp. 1097-1104.

7 **Cubrinovski M.**, **Ishihara K.**, Maximum and minimum void ratio characteristics of sands, *Soils and Foundations,* **2002**, **42**(6), pp. 65-78.

8 **Biarez J.**, **Hicher P.-Y.**, *Elementary mechanics of soil behaviour, saturated remoulded soils*, Balkema, Rotterdam, **1994**, 207 pages.

9 **Fuller W.B.**, **Thompson S.E.**, *The laws of proportioning concrete*, Trans. american society of civil engineers (ASCE), **1907**, **59**, pp. 64-143.

10 **De Larrard F.**, *Structure granulaire et formulation des bétons*, **2000**, ERLPC, OA34, 414 pages

11 **Cola S.**, *On modelling the behaviour of melanges, Numerical methods in geotechnical engineering*, Mestat (ed.), Presses de l'ENPC/ LCPC, Paris, **2002**, pp. 134-138.

12 **Omine K.**, **Ochai H.**, **Yoshida N.**, Deformation-strength properties of intermediate soils under triaxial conditions, *Proceedings of the international symposium on pre-failure deformation of geomaterials*, (2) Shibuya *et al.* (eds.), Balkema, **1994**, pp. 407-413.

13 **Kézdi Á.**, Problems in soil physics, conférence prononcée devant l'université autonome de Mexico, *Sociedad mexicana de mecanica de suelos*, **1976**, 69 pages.

14 **Hussain B.**, **Katti R.K.**, Behaviour of soil rock mixtures in shear and compression, *International symposium on landslides*, New Delhi, **1980**, volume **1**, pp. 113-117.

15 **Mvondo-Ondoa J.**, *Rôle de la granularité et de la composition minéralogique sur la compactabilité et la résistance au cisaillement des mélanges de sable et d'argiles*, Thèse de doctorat de l'École nationale supérieure des mines de Paris et Paris VI, **1979**, 150 pages.

16 **Holtz W.G.**, **Gibbs H.J.**, Triaxial shear tests on pervious gravelly soils, *Journal of soil mechanics and foundations division,* ASCE, **1956**, **82**(SM1), pp. 867.1-867.22.

17 **Holtz W.G.**, Some thoughts about index properties for evaluating the mechanical properties of rockfill and gravel materials, Contribution and discussion on mechanical properties of rockfills and gravel materials, *Proceedings of the 7th international conference on soil mechanics and foundation engineering*, Mexico, **1969**, pp. 127-132.

18 **Verdeyen J.**, **Roisin V.**, *Stabilité des terres, sols routiers, soutènements, talus,* Édition Eyrolles, **1956**, 420 pages.

19 **Holtz W.G.**, **Ellis W.**, Triaxial shear characteristics of clayey gravel soils, *Proceedings of the 6th international conference on soil mechanics and foundation engineering*, Montréal, **1965**, volume **1**, pp. 143-149.

20 **Road Research Laboratory**, *Soil Mechanics for road engineers*, Her Majesty's stationery office, **1952**, 541 pages.

21 **Fragaszy R.J.**, **Su J.**, **Siddiqi F.H.**, **Ho C.L.**, Modelling strength of sandy gravel, *Journal of geotechnical engineering*, ASCE, **1992**, **118**(6), pp. 920-935.

22 **Gibson R.E.**, Experimental determination of true cohesion and true angle of internal friction in clays, *Proceedings of the 3rd international conference on soil mechanics and foundation engineering*, Zurich, **1953**, vol. **1**, pp. 126-130.

23 **Terzaghi K.**, **Peck R.B.**, *Soil mechanics in engineering practice*, a Wiley International Edition, **1967**, 729 pages.

24 **Nahum M.**, *Étude des sols hétérogènes*, rapport interne LCPC, **2003**, 37 pages.

25 **Nguyen Pham P.T.**, *Étude analytique de l'essai triaxial avec des mélanges de plusieurs composantes, comparaison avec les résultats expérimentaux*, rapport interne LCPC, **2004**, 45 pages.

26 **Favre J.-L.**, **Biarez J.**, **Mekkaoui S.**, 2002, Modèles de comportement en grandes déformations des sables et argiles remaniées à l'œdomètre et au triaxial, *Symposium international sur l'identification et la détermination des paramètres des sols et des roches pour les calculs géotechniques*, Paris, **2002**, Magnan (ed.) Presses de l'ENPC/LCPC*,* pp. 369-384.

27 **Serratrice J.-F.**, **Reiffsteck Ph.**, Typologie de la forme des chemins non drainés à l'appareil triaxial, *Symposium international ELU-ULS géotechnique*, Paris, **2006**, Droniuc, Magnan et Mestat (ed.) Édition LCPC.

28 **McGeary R.K.**, Mechanical packing of spherical particles*, Journal of american ceramic society*, **1961**, vol. **44**, n° **10**, pp. 513-522.

29 **Reiffsteck Ph.**, **Blivet J.-C.**, **Vallé N.**, **Khay M.**, Écueils de la mesure en laboratoire du comportement mécanique des sols grossiers, *15th International conference on soil mechanics and foundation engineering*, Istanbul, Balkema, **2001**, pp. 255-259.

30 **Vallé N.**, *Propriétés mécaniques d'un sol grossier d'une vallée alluvionnaire de la Seine*, Thèse de doctorat de l'Université de Caen, **2001**, 297 pages.

31 **Burminster D.M.**, Principles of permeability testing of soils, *Symposium on permeability of soils*, Chicago, **1954**, ASTM STP163, pp. 3-20.

32 **Nguyen T.-D.**, **Fleureau J.-M.**, **Modaressi A.**, Identification of parameters and validation of Hujeux model for a coarse soil, International association of computer methods and advances in geomechanics (IACMAG), Turin, **2005**, pp. 433-440.

33 **Mitchell J.K.**, *Fundamental of soil behavior*, Series in soils engineering, John Wiley & Sons Inc., **1976**, 422 pages.

34 **Roscoe K.H.**, **Burland J.B.**, *On the generalised stress-strain behaviour of 'wet'clay*, in J. Heyman and F.A. Leckie (eds.), Engineering plasticity, Cambridge Univer. Press, **1968**, pp. 535-609.

35 **Mestat Ph.**, *Lois de comportement des géomatériaux et modélisation par la méthode des éléments finis*, **1993**, ERLPC, GT52, 193 pages.

36 **Dupla J.-C.**, **Pedro L.-S.**, **Canou J.**, **Dormieux L.**, Comportement mécanique des sols grossiers de référence, *Bulletin des laboratoires des ponts et chaussées*, **2007**, **268-269**, pp.

37 **Arbaut J.**, *Caractérisation mécanique des sols hétérogènes*, Mémoire de MASTER CNAM, **2007**.

38 **Shirdam R.**, *Comportement mécanique des matériaux superficiels des versants naturels*, Thèse de doctorat, Institut national des sciences appliquées de Lyon, **1998**.